Effects of inversion asymmetry on electron energy band structures in GaSb/InAs/GaSb quantum wells

J. Luo*
Department of Physics, Brown University, Providence, Rhode Island 02912

H. Munekata and F. F. Fang
IBM Research Division, Thomas J. Watson Research Center, P.O. Box 218, Yorktown Heights, New York 10598

P. J. Stiles
Department of Physics, Brown University, Providence, Rhode Island 02912
(Received 25 September 1989)

We report experimental evidence that indicated the lifting of the spin degeneracy of the two-dimensional (2D) electron ground subband due to the lack of inversion symmetry in narrow InAs/GaSb quantum wells. Through detailed analysis of the beating patterns in 2D electron Shubnikov–de Haas (SdH) oscillations, we conclude that the finite spin splitting at $B=0$ is dominated by the lack of inversion symmetry in the confining potential well. The effects of the inversion asymmetry connected with the InAs bulk structure, although they exist, are of minor importance in the samples studied. The 2D energy band structure in such asymmetric wells can be described by including the Rashba term, $H_{s.o.}=\alpha_s(\boldsymbol{\sigma}\times\mathbf{k})\cdot\mathbf{z}$, into the electron Hamiltonian; the spin-orbit coupling constant $\alpha_s=0.9\times10^{-9}$ eV cm is determined for a 75-Å well by simulating the measured SdH oscillations. We also studied the magnetic field dependence of the spin splitting by rotating the sample in constant magnetic fields as high as 15 teslas. The results indicate that the spin splitting increases nonlinearly with the external magnetic field. Finally, the electron scattering times of the two spin states of the ground electron subband are not always the same; their difference is found to increase with the spin splitting. The possibility of spin-dependent scattering mechanisms is also discussed.

I. INTRODUCTION

The electron states in an ideal noninteracting two-dimensional electron gas (2DEG) are twofold spin degenerated unless an external magnetic field **B** is applied. The magnetic-field-induced spin splitting, the so-called Zeeman term, is equal to $g\mu_B B$, with μ_B the Bohr magneton and the free-electron spin g factor of about 2. This description, however, is too simple for most real 2DEG systems because not only do the electrons strongly interact with each other, they also are influenced by electronic properties of their host system. One of the most extensively studied 2DEG systems is an inversion layer on a Si metal-oxide-semiconductor field-effect transition (MOSFET). The spin splitting of the 2D energy levels in the inversion layer can be properly described by the Zeeman term; but the spin g factor has been shown to depend on the electron concentration and on the position of the Fermi energy relative to the Landau levels due to many-body effects.[1] If the host system lacks spatial inversion symmetry, then the spin degeneracy of 2D electron states is lifted even in the absence of an external magnetic field. Effects related to this zero-field spin splitting have been reported recently in systems such as GaAs,[2] $In_xGa_{1-x}As$,[3] and $Hg_xCd_{2x}Te$.[4]

In this paper, we report an experimental study of molecular-beam-epitaxy (MBE)-grown InAs/GaSb quantum wells which contain a 2DEG confined in the InAs layer sandwiched between two GaSb barriers. An interesting feature of the InAs/GaSb system is that the electrical properties of the 2DEG strongly depend on the InAs layer width (d_z). The wide wells ($d_z>100$ Å) exhibit well-defined Shubnikov–de Haas effects. The electron spin splitting depends linearly on the external magnetic field and vanishes at $B=0$; the g factor varies in general from the InAs bulk value of 15 and decreases with reducing of the well width. For example, values of $g=19$ and 17 have been measured by Chang *et al.*[5] on InAs/GaSb superlattices with $d_z=1000$ and 500 Å, respectively, and $g=8$ measured on 100-Å wells by Smith and Fang.[6] The dependence of g factor on the well width is attributed to the competing effects of electron many-body interactions and the InAs conduction-band nonparabolicity in the system. Many-body effects enhance the spin g factor for decreasing electron density in a similar fashion to that observed in Si inversion layers. The nonparabolicity effects, which are negligible in Si but become rather important for InAs, tend to reduce the g factor for increasing confinement energy. Therefore, reducing the well width can effectively enhance the effect of nonparabolicity and to cause the g factor to become smaller than the InAs bulk value. In extremely thin wells ($d_z\sim75$ Å), the SdH oscillations show beating patterns instead of the usual simple $1/B$ periodic oscillations due to the finite

zero-field spin splitting of the ground electron subband.[7] The focus of this work is on this group of extremely narrow InAs/GaSb quantum wells, i.e., to identify the origin of the zero-field spin splitting and to study the evolution of the spin splitting in finite external magnetic fields.

II. THE ORIGIN OF THE ZERO-FIELD SPIN SPLITTING

The zero-field spin splitting of electron energy levels in a quantum well can be caused by the lack of inversion symmetry either in the host semiconductor bulk crystal potential or in the interface confinement potential. Both kinds of asymmetry exist in the InAs/GaSb system studied here because InAs, with a zinc-blende structure, is intrinsically inversion asymmetric, and a certain degree of asymmetry in the potential well is also expected due to the characteristics of the growth of the samples. The spin splitting of Γ_6 conduction band in a bulk zinc-blende semiconductor has been ascribed to a k^3 contribution in conduction-band Hamiltonian.[8] When a quantum well is built on this type of semiconductor, the electron wave vector perpendicular to the layer is quantized to $k_z \sim (\pi/d_z)$ and the electrons can only move freely along the well plane. If the quantum well is thin enough that the in-plane wave vector $k \ll (\pi/d_z)$, then the spin splitting caused by the bulk asymmetry will be dominated by the leading term

$$\Delta_{\text{bulk}} \sim \gamma \left[\frac{\pi}{d_z} \right]^2 k \ , \tag{1}$$

where k is the in-plane 2D wave vector and γ is a material-specific constant.[9] The well-width-dependent coefficient $(\pi/d_z)^2$ indicates that the spin splitting that originated from the bulk inversion asymmetry can be enhanced by the quantum confinement.

The spin splitting associated with the potential-well asymmetry, on the other hand, has no explicit dependence on the well thickness. An asymmetric well is accompanied by an interface electric field, which is directed along the normal of the well plane and lifts the spin degeneracy of the 2D electron energy bands by coupling the electron spin and orbital motion. This spin-orbital coupling is described by a Hamiltonian[10,11] $H_{\text{s.o.}} = \alpha_s (\boldsymbol{\sigma} \times \mathbf{k}) \cdot \mathbf{z}$, where $\boldsymbol{\sigma}$ is the vector of the Pauli spin matrices, $\mathbf{z}$ is the unit vector along the surface field direction, and $\mathbf{k}$ is the electron wave vector along the plane. The spin-orbit coupling constant α_s is implicitly proportional to the strength of the built-in surface electric field (E_{surf}). Since it was first introduced by Rashba, this spin-orbit Hamiltonian $H_{\text{s.o.}}$ is usually referred to as the Rashba term. The resultant spin splitting,

$$\Delta_{\text{s.o.}} \sim E_{\text{surf}} k \ , \tag{2}$$

is proportional to the Fermi wave vector and the strength of the surface electric field. Because of variations during the MBE growth of the InAs/GaSb quantum wells used in our experiments, the degree of potential-well asymmetry, and therefore the surface-field-induced spin splitting, varies from sample to sample independent of the well thickness.

The two aspects of the total spin splitting, that caused by the bulk structure and that by the interface potential, are both proportional to the electron in-plane wave vector. No matter which one of them dominates, the sample with higher electron concentration (n_s) exhibits larger zero-field spin splitting in the SdH-type measurements that probe the electronic properties at the Fermi level. This is because the Fermi wave vector $k_f = (2\pi n_s)^{1/2}$ for a 2D system. The evaluation of the bulk or surface field term based on the total spin splitting obtained for a given sample is nearly impossible due to the lack of quantitative information about either one of them. Because of the $(1/d_z)^2$ dependence of the bulk asymmetry term, however, samples with comparable carrier concentrations but with different well widths can be examined to give a quick insight into the relative importance of the bulk and well asymmetry effects.

Devices consisting of a 75- or 100-Å InAs layer were examined for this purpose. The samples, with a typical electron mobility of $\sim 20\,000$ cm^2/V s at 4.2 K, were grown from identical material following the same MBE procedures. We have chosen two wells with similar electron concentrations: 1.0×10^{12} cm^{-2} for the 75-Å well and 1.14×10^{12} cm^{-2} for the 100-Å well. Because of the InAs conduction-band nonparabolicity effects, their effective electron masses at the Fermi energy are slightly different from each other with $0.055 m_0$ for the narrower well and $0.047 m_0$ for the wider well. Here, m_0 is the free electron mass. If the bulk asymmetry term dominates, then the zero-field spin splitting of the 100-Å well would be approximately $(75/100)^2 \sim 0.6$ times smaller than that of the 75-Å well. This could be tested by a simple analysis of the beating pattern in the SdH oscillation from the two samples.

Figure 1 shows the magnetoresistivity ρ_{xx} at 1.2 K as a function of the magnetic field applied perpendicular to the 2D layer. The low-field SdH oscillations shown in the insets are quite different for the two samples, both in the number of oscillations between the beat minima, usually called nodes, and in the oscillation amplitude at the nodes. The nonzero amplitude at the node of the 100-Å sample indicates that the electrons in the two spin subbands oscillate at different strength, and a detailed discussion of this will be given in a later section. Here we focus on the spin splitting, which is inversely proportional to the number of oscillations between two adjacent nodes when the total number of electrons is held constant.[7] Clearly shown in the insets of Fig. 1 is that the 100-Å well has $N^{(100\ \text{Å})} = 3$ oscillations between the nodes [Fig. 1(a)], and the number is $N^{(75\ \text{Å})} = 11$ for the 75-Å well [Fig. 1(b)]. Thus, the ratio of the zero-field spin splitting between the two samples is given by the following:

$$\Delta_{\text{spin}}^{(100\ \text{Å})} / \Delta_{\text{spin}}^{(75\ \text{Å})} = N^{(75\ \text{Å})} / N^{(100\ \text{Å})} = 11/3 \sim 4 \ . \tag{3}$$

Therefore the zero-field spin splitting of the wide well (100 Å) is much larger than that of the thin well (75 Å), contrary to the expectation from the bulk structural asymmetry term. On the other hand, this result can be easily fitted into the well asymmetry picture by assuming

a stronger surface electric field in the 100-Å device. So we conclude that we have observed the zero-field spin splitting caused by the spin-orbital coupling associated with the well asymmetry, and the contribution from bulk asymmetry is effectively negligible.

III. ENERGY LEVELS OF 2DEG WITH SPIN-ORBIT INTERACTION

In this section we study the effects of the inversion asymmetry on the 2D electron energy levels by simulating the measured SdH oscillations. The magnetoconductivity of a two-dimensional electron gas at $T=0$ K is given by[12]

$$\sigma_{xx}=\frac{e^2}{\pi^2\hbar}\sum_{n\pm}(n\pm\tfrac{1}{2})\exp\left[-\frac{(E_f-E_{n\pm})^2}{\Gamma^2}\right], \tag{4}$$

where E_f is the Fermi energy and $E_{n\pm}$ is the energy of the nth Landau level with spin up (+) or down (−). Here the Landau-level broadening Γ has been assumed to be a constant, i.e., independent of the Landau-level index.

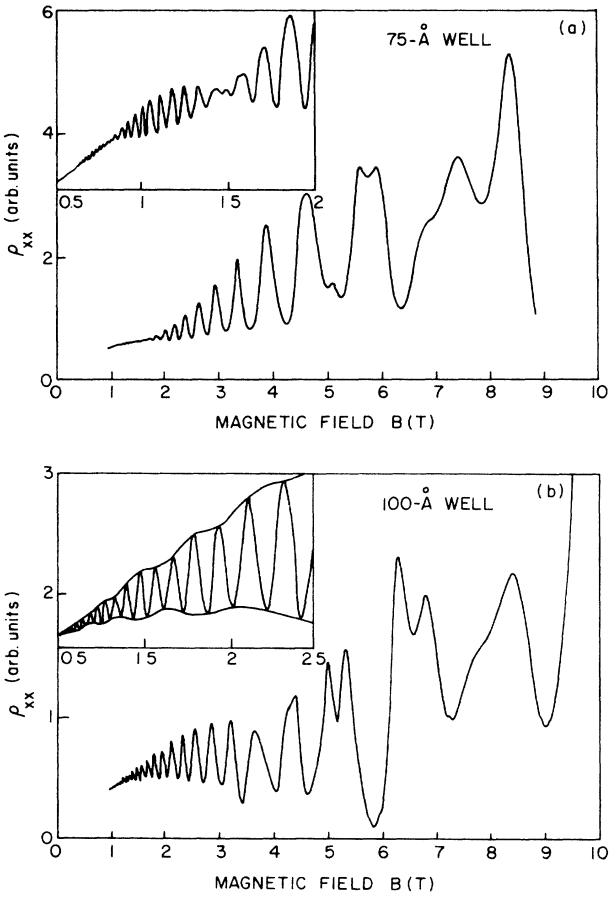

FIG. 1. The magnetoresistance as a function of the magnetic field applied perpendicular to the well plane at 4.2 K. The insets show the low-field SdH oscillation detail that leads to the evaluation of the zero-field spin splitting: the data from the 75-Å well (a) have 11 oscillations between two adjacent beat nodes; the number is 3 for the data from the 100-Å well (b).

For quantizing magnetic fields ($\sigma_{xy}^2 \gg \sigma_{xx}^2$) the transverse resistivity ρ_{xx} is given as

$$\rho_{xx}=\sigma_{xx}/(\sigma_{xy}^2+\sigma_{xx}^2)\simeq\sigma_{xx}/\sigma_{xy}^2\simeq\sigma_{xx}(B/en_s)^2 . \tag{5}$$

Equation (4) shows clearly that the measured SdH oscillation in ρ_{xx} reflects directly the Landau-level spectrum of the system: it reaches its maximum, or its minimum, depending on whether the Fermi energy is near the center of the Landau levels, or is between two Landau levels, respectively.

Different models for the Landau levels have been tested. For a given set of Landau levels ($E_{n\pm}$), we first calculate the Fermi energy by solving an integral equation which relates E_f to the measured 2D electron density:[13]

$$n_s=\int_0^\infty \mathcal{N}^{2D}(E)f(E,E_f,T)dE , \tag{6}$$

where $f(E,E_f,T)=1/\{1+\exp[(E_f-E)/kT]\}$ is the Fermi distribution function. The 2D density of states is assumed to be of a Gaussian line shape:

$$\mathcal{N}^{2D}(E_{n\pm})=\frac{1}{2\pi l^2}\sum_{n\pm}\frac{1}{\Gamma}\left[\frac{2}{\pi}\right]^{1/2}\exp\left[-2\frac{(E_f-E_{n\pm})^2}{\Gamma^2}\right], \tag{7}$$

where $l=(\hbar c/eB)^{1/2}$ is the magnetic length. Using the solution of the Fermi energy as a function of magnetic field, we then calculate ρ_{xx} by using Englert's formula (4) together with Eq. (5). The value of Γ and the parameters in the Landau spectrum $E_\pm$ are adjusted to minimize the deviation between the simulation and the experimental data. Our numerical calculations are limited to zero temperature since the consideration of finite temperature is found to be of minor importance at 1.2 K.

A. Constant spin-splitting model

We started with a simple model that assumes the only effect of the spin-orbit interaction is to introduce a constant spin splitting to the ground electron subband. The electrons in these two spin bands are then treated as two independent free 2D electron gases. The zero magnetic field energy dispersion $E(k)$ and the Landau-level spectrum $E_{n\pm}$ in a finite perpendicular magnetic field B are given, respectively, by

$$E(k)=\frac{\hbar^2k^2}{2m}\pm\tfrac{1}{2}\Delta_{\text{spin}} , \tag{8}$$

$$E_{n\pm}=(n+\tfrac{1}{2})\hbar\omega_c\pm\tfrac{1}{2}\Delta_{\text{spin}},\quad n=0,1,2,\ldots , \tag{9}$$

where $\hbar\omega_c=eB\hbar/mc$ is the Landau-level separation and Δ_{spin} is the spin splitting. This model is illustrated graphically in Fig. 2, with the Landau levels shown in the main window and the dispersion at $B=0$ appearing in the inset.

Although not explicitly stated in the previous section, the derivation of the zero-field spin splitting by counting the number of oscillations between the nodes is actually based on this model. This is because the assumption that the two frequency components in the SdH oscillations are sinusoidal with fixed relative frequency is only valid if the

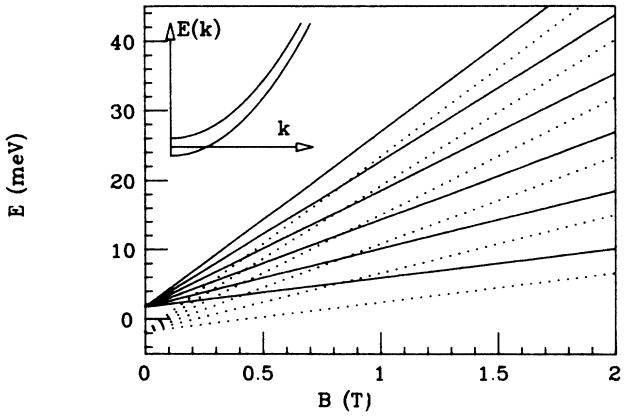

FIG. 2. Energy spectrums from the constant spin splitting model: the energy dispersion (inset) and the Landau-level spectrum (main curve).

spin splitting is a constant. The magnetoresistivity calculated on the basis of this energy-level scheme exhibits a beating pattern that is most sensitive to the value of Δ_{spin} which determines the number of oscillations between the beat nodes. The best fit to the experimental data from the 75-Å well is achieved with $\Delta_{spin}=3.7$ meV. For easier comparison, only the oscillatory part of ρ_{xx} is presented in Fig. 3 for both the simulation result and the data.

The simulation based on the constant spin-splitting model captures the essential features of the experimental beat pattern (the number of the oscillations between the beat nodes is identical to the data), but it fails to give the correct beat node position (simulated oscillations are somehow shifted in B field with respect to the experimental data). The existence of such a discrepancy is not surprising because the electron energy spectrum is actually more complicated than this constant spin-splitting model, particularly in the small-k region.

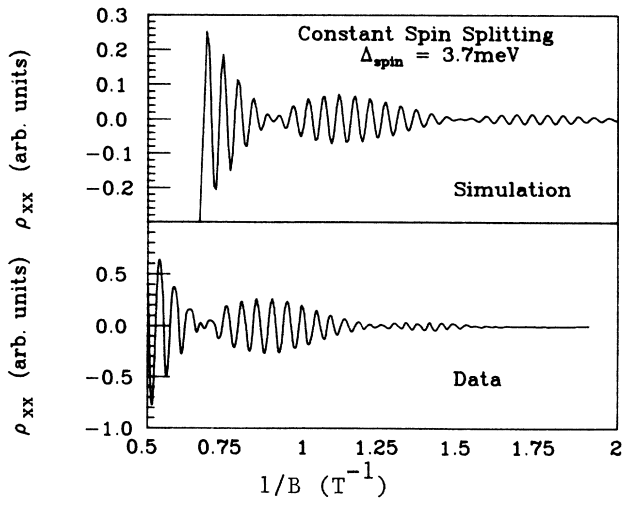

FIG. 3. Numerical simulation for the magnetoresistance oscillation from the 75-Å well with the constant spin-splitting model. The best value for the spin splitting is $\Delta=3.7$ meV.

B. Rashba model

According to Bychkov and Rashba,[11] the exact solution to the Hamiltonian

$$H=\hbar^2k^2/2m+\alpha_s(\sigma\times\mathbf{k})\cdot\mathbf{z} \tag{10}$$

yields the electron energy dispersion related to the motion along the 2D plane:

$$E(k)=\frac{\hbar^2k^2}{2m}\pm\alpha k\ . \tag{11}$$

The important characteristic of this dispersion relation is that the spins are degenerate at $k=0$ and the spin splitting linearly increases with k. The Landau spectrum in the magnetic field perpendicular to the 2D layer is given by

$$\begin{aligned} E_{n\pm}&=\hbar\omega_c[n\pm(\delta^2+\gamma^2n)^{1/2}],\\ E_0&=\hbar\omega_c\delta,\quad n=1,2,3,\ldots\ , \end{aligned} \tag{12}$$

where $\delta=[1-gm/(2m_0)]/2$ and $\gamma=(2m\alpha_s^2/\omega_c)^{1/2}$.

Figure 4 shows the schematic electron energy spectrums calculated from the Rashba model with an exaggerated spin-orbital coupling constant α_s. The spin-orbit interaction clearly causes the Landau levels to become highly nonlinear due to accumulative effect of low-energy electron states in the subband. The most important parameter in this model is α_s, which measures the strength of the spin-orbit coupling. Shown in dashed lines in Fig. 5 is the simulation with the parameters $\Gamma=1.5$ meV, $g=10.5$ and $\alpha_s=0.9\times10^{-9}$ eV cm. It should be noted that the Landau levels $E_{n\pm}$ are different from Fig. 4 if the bulk asymmetry term, instead of the Rashba term, is included in the calculation.[4] Thus, the very good agreement between the experimental data and the numerical simulation in Fig. 5 provides further evidence that the surface-field-related spin-orbit interaction indeed dominates over the bulk term in the InAs/GaSb system stud-

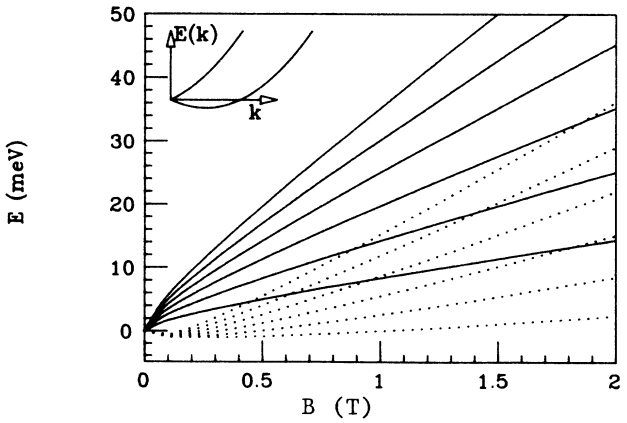

FIG. 4. The energy spectrum of Rashba's model. The spin-orbital coupling constant α_s used in the calculation has been exaggerated to show the nonlinearity of the Landau level. One important difference from the constant spin-splitting model of Fig. 2 lies in the fact that the two spin states are degenerate at $k=0$ in the Rashba model.

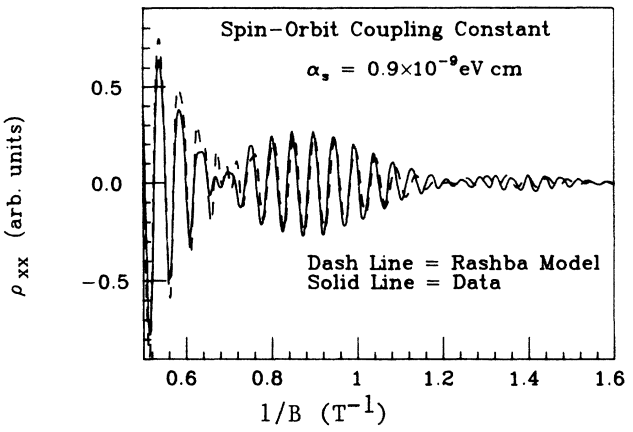

FIG. 5. Numerical simulation (dashed lines) for the magnetoresistance oscillation from the 75-Å well (solid lines) with Rashba's model. The parameters used in the calculation are the spin-orbit constant $\alpha_s = 0.9 \times 10^{-9}$ eV cm, and the level broadening $\Gamma = 1.5$ eV.

ied here. Bychkov and Rashba[11] have determined the spin-orbit coupling constant α_s for the experimental data on GaAs heterojunctions by Stein *et al.* (electron-dipole spin transitions) and Störmer *et al.* (cyclotron resonances). Their values are $\alpha_s \sim 2.5 \times 10^{-10}$ eV cm for the 2D electrons and $\alpha_s \sim 0.6 \times 10^{-9}$ eV cm for the 2D holes. The spin-orbital coupling constant obtained here is larger than that of GaAs heterojunctions, in part indicating stronger spin-orbit interaction in InAs material and/or reflects the many-body effect enhancement of g factor in SdH measurements.

Based on the numerical simulation results, we concluded that the 2D electrons in InAs/GaSb quantum wells are best described by the type of energy dispersions shown in Fig. 4. It should be noticed that in Rashba model the spin-orbital coupling constant α_s is the only variable and the zero-field spin splitting does not enter the calculation. The zero spin splitting at the Fermi level in Rashba's model is given by $2\alpha_s k_f$, with k_f the average Fermi wave vector determined by the total number of electrons in the system. From the known $\alpha_s \sim 0.9 \times 10^{-9}$ eV cm and the total electron concentration $n_s = 1.0 \times 10^{12}$ cm^{-2}, $2\alpha_s k_f = 4.0$ meV is obtained. This value is in reasonable agreement with $\Delta_{\text{spin}} = 3.7$ meV obtained by counting the number of oscillations between beat nodes (i.e., the constant spin-splitting model). Therefore, for the energy analysis purpose, the constant spin-splitting model is still acceptable. The origin of the phase shift in the simulation based on the constant spin-splitting model becomes rather clear by comparing the energy levels in Fig. 2 with those in Fig. 4. The Landau-levels spectrum from the constant spin-splitting model varies from the Rashba model, most obvious in the low-field region, causing an error in predicting the positions of the Landau-level position in the magnetic field at the Fermi energy. Since the complete consideration of the Landau-level spectrum in a tilted magnetic field becomes extremely complicated, we will use the constant spin-splitting model in the following discussion of the evolution of the spin splitting in a tilted magnetic field.

IV. MAGNETIC FIELD DEPENDENCE OF THE SPIN SPLITTING

Since the SdH measurement is a finite magnetic field probe, the zero-field spin splitting obtained from analyzing the beat pattern is really the averaged spin splitting in the beat field window, for example, about 0.5–1.5 T for the 75-Å well. However, since the Zeeman splitting is negligible in such small magnetic fields, the total spin splitting is dominated by the contribution from the surface electric field term, providing a good approximation for the spin splitting at $B \to 0$. In this section we employed the tilting field technique of Fang and Stiles[14] to study the spin splittings of the 2D EG over a larger magnetic field range.

The basic assumption for applying the tilting field technique is that the electron spin splitting is determined by the total magnetic field, while the Landau-level separation is determined by the field component perpendicular to the 2D layer. For a 2D EG with strong spin-orbit coupling, one might expect the spin splitting to depend on the magnetic field (both magnitude and orientation) in a more complicated way. However, the spin splitting is found to be fairly constant for all tilting angles in the study by Radantsev *et al.*[15] on the $Hg_xCd_{1-x}Te$ heterostructures, another material with strong spin-orbit coupling. This indicates that the tilted field technique can be applied to the InAs system under consideration.

In the following measurements we rotate the sample in a constant magnetic field B_t. The Landau-level separation varies with the tilting angle θ as it is determined by the magnetic field perpendicular to the 2D plane, by $B_\perp = B_t \cos(\theta)$. The spin splitting, on the other hand, is undisturbed by the rotation. The measured SdH oscillation (ρ_{xx} versus $B_\perp$) yields information about the electron concentrations of the two spin states, and hence, the spin splitting at that particular total field. In evaluating the electron spin splitting, we use a constant cyclotron mass of $0.055 m_0$ for all tilting angles. Because of the nonparabolic InAs conduction band, the electron effective mass would increase with the total magnetic field, which may raise the electron Fermi level through the diamagnetic energy shift of the subband. However, such nonparabolicity effect is extremely small since the Fermi energy tends to be pinned at the interface. A detailed discussion of the diamagnetic energy and the Fermi energy pinning will be given in Sec. IV B.

A. Beating patterns in $B_t < 8$ T

The magnetoresistivity ρ_{xx} is recorded at 1.2 K as a function of the tilting angle for 15 different total magnetic fields ranging from 2 to 15 T. One set of these oscillations for the 75-Å well is plotted against the inverse of the normal magnetic field component $1/B_\perp$ in Fig. 6. The beat node positions along with N, the number of oscillations between them, are also indicated. For easier identification of the nodes position, the smooth back-

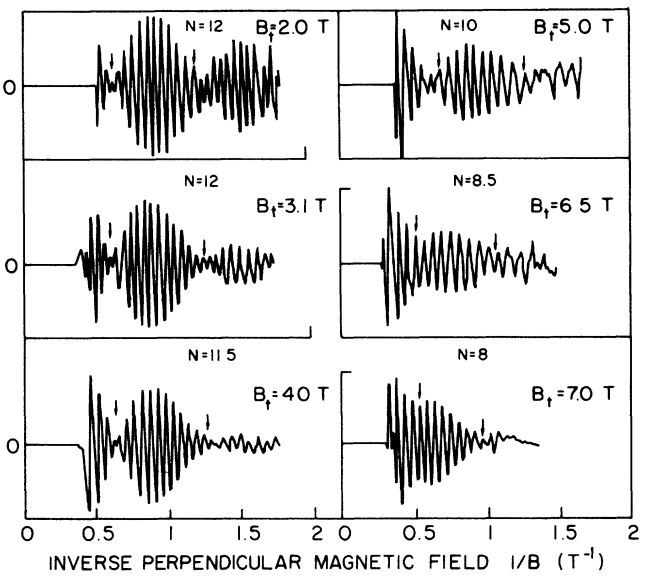

FIG. 6. The evolution of the beating pattern from the 75-Å well in tilted magnetic fields up to 7.0 T. With increasing total magnetic field, the number of oscillations between the beat nodes decreases while the beat node opens up—oscillation amplitude at the node increases.

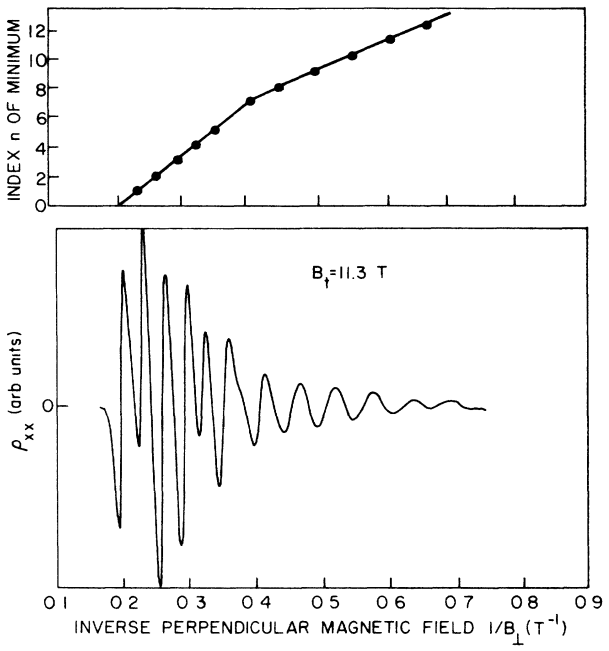

FIG. 7. The beating pattern is not observed if the total magnetic field is higher than 8.0 T, because the electron scattering times become so different that only one spin contributes to the oscillations in small $B_\perp$ field. The figure shows the SdH oscillation at $B_t = 11.3$ T as an example. In this case, the electron concentrations of the two spin states can be determined from the slopes of the index of the oscillation maximum vs $1/B_\perp$ plot.

ground in each trace of ρ_{xx} versus $1/B_\perp$ has been subtracted. Presented here are the oscillatory parts multiplied by an exponential factor $e^{B_0/B_\perp}$, with $B_0 = 3.25$ T on the average, to roughly compensate the field decay of the oscillation amplitude. The level broadening Γ can be evaluated from the characteristic field B_0 by setting the collision damping of the SdH oscillation[1] $\exp(-2\pi\Gamma/\hbar\omega_c) = \exp(-B_0/B_\perp)$. The value obtained, $\Gamma = 1.5$ meV, is consistent with that assumed in the simulation of the beating pattern in the previous section.

The data in Fig. 6 show that with increasing total magnetic field the amplitude at the beat node increases, or in other words, the SdH amplitudes from the two spin states grow increasingly apart from each other. Unequal scattering times for the two spin states have to be provoked to explain this behavior, and the details will be discussed in a later section. As for the spin splitting $\Delta_{\text{spin}} \sim 1/N$, the trend is very clear that it is essentially independent of the strength of the total magnetic field at $B_t < 4.0$ T and increases with B_t beyond this field.

B. Beating patterns in $B_t > 8T$

Another set of the tilted field SdH oscillations are measured in total magnetic field higher than 8.0 T. As the beat pattern in Fig. 6 continues to evolve with the increasing total magnetic field, the scattering rates of the two spin states become so different from each other that only one spin contributes to the SdH oscillation at low quantizing field; the other spin state starts to oscillate at a much higher field. The oscillatory behavior of ρ_{xx} at $B_t = 11.3$ T is shown in Fig. 7 as an example of this group of data. Instead of beating pattern, the data are best characterized by a frequency switch in the otherwise "normal" sinusoidal oscillations in $1/B_\perp$ field. The transition quantizing field is indicated by the intersection of the two straight lines in the plot of the field positions of oscillation maxima versus their indexes. The section-wise linear index plot can be used to our advantage in determining the electron concentrations of the two spin bands, because the slope of an index plot is directly proportional to the number of electrons participating in the oscillation. The electron concentration of the spin with the long scattering time, $n_1 = 4.5 \times 10^{11}$ cm^{-2}, is given by the slope of low $B_\perp$ region, and the total electron concentration, $n_{\text{total}} = 8.1 \times 10^{11}$ cm^{-2}, is given by the slope in the high $B_\perp$ region where both bands participate in the oscillation. Finally, the electron concentration for the spin with the short scattering time, $n_2 = n_{\text{total}} - n_1 = 3.6 \times 10^{11}$ cm^{-2}, is easily obtained.

The following features emerge from a close examination of this high-field data shown in Fig. 7. First, the spin splitting indeed has no field orientation dependence because otherwise the charge transfer would occur between the two spin levels following the sample's rotation and the index curve would not be linear. Secondly, since the spin state with the long scattering time has more electrons, i.e., $n_1 > n_2$, it is lower in energy. Finally, the system lost $\delta n_{\text{lost}} = n_0 - n_{\text{total}}$ electrons from the well during the tilting, where $n_0 = 1.0 \times 10^{12}$ cm^{-2} is the electron concentration obtained from low-field Hall measurement. The missing electrons can be accounted for by considering the diamagnetic shift of the ground-state energy, which is the rise of the 2D electron subband energy due

to the shifting of cyclotron orbit centers in a parallel magnetic field. Normally diamagnetic energy is undetected by transport measurements because the Fermi energy also moves up by the same amount along with the 2D electron subband so that the relative energy between the two levels is not changed. In the InAs/GaSb quantum wells there exist some positively charged states in the GaSb sides, whose energies are above the initial electron Fermi energy. As the diamagnetic shift raises Fermi level across these charge states, they are occupied by electrons from the well and become neutralized. The diamagnetic energy is estimated to be $E_{\rm diam}=e^2B_{\parallel}^2\langle z_{nn}^2\rangle/2m\approx 13$ meV, assuming the standard derivation of electron wave function z_{nn} equal to the well width 75 Å and parallel field $B_{\parallel}\simeq B_t=11.3$ T for the experimental regime of the tilting angle. Since the actual shift of the Fermi level could be anywhere between zero and $E_{\rm diam}$, the value $p_{\rm surf}=\delta n_{\rm lost}/E_{\rm diam}=1.2\times 10^{13}$ cm^{-2} eV^{-1} gives the lower limit for the density of states of the positive charges in the GaSb barrier. The quantum well is asymmetric due to the uneven distribution of these charge states among the two GaSb barriers.

The electron concentrations of the two spin bands and the spin splitting at $B_t=8.0$, 9.0, and 10.0 T are also determined by measuring the two slopes of the index plot. The data in field higher than 11.3 T are not used because our tilting apparatus has an angle resolution of 1° and the resulting error bar in our calibration of the perpendicular field becomes excessive at large tilting angles. Although a different approach—counting the number of oscillations between the adjacent beat nodes—has been applied to the carrier concentration analysis of the tilted field data for $B_t<8$ T, where the beat is the main characteristic of the SdH oscillations. The two groups of tilting field data, despite their strikingly different line shapes, are in fact the same type of SdH oscillations that consist of the contributions from two electron bands.

C. Spin splitting versus B_t

The results of $\Delta_{\rm spin}$ versus B_t are summarized in Fig. 8, where the low- and high-field sections join smoothly around $B_t=8.0$ T, although the methods of obtaining $\Delta_{\rm spin}$ in the two regimes are quite different as discussed above. Thus, the spin splitting is a smooth function of the magnetic field despite the apparently abrupt changes in the SdH oscillation line shape. The uncertainties in $\Delta_{\rm spin}$ are due to the limited accuracy of $\pm 1°$ in the calibration of the rotating angle θ.

The results in Fig. 8 clearly demonstrate how the spin splitting evolves as the external magnetic field increases: the spin splitting remains at its zero-field value in the magnetic field up to 5.0 T, then it starts to increase. The characteristics of this result can be easily understood if one views the built-in surface electric field as an equivalent magnetic field in the electrons' rest frame of reference. When the external magnetic field is small compared with the strength of this internal field, the total electron spin splitting is basically determined by the spin-orbital coupling effects. Hence it has little dependence on the external magnetic field. The spin Zeeman splitting becomes more important with increasing external field strength and eventually causes the later increase of spin splitting as observed at high fields. The dashed lines in Fig. 8 show the field dependence of the Zeeman splitting $g\mu_B B$, for $g=19$ obtained by Chang *et al.*,[5] and for $g=8$ obtained by Smith and Fang.[6] In both experiments no zero-field spin splitting was reported presumably because the quantum wells examined were considerably more symmetrical than ours. Our results shown in Fig. 8 are consistent with the rms value of the zero-field splitting term and the Zeeman term of Smith and Fang for data below 9 T. For higher magnetic field, the observed spin splitting is likely enhanced by the many-body exchange interaction. The $g=19$ result of Chang *et al.* was observed in much wider quantum wells (15–100 nm) where the nonparabolicity effect reported in Ref. 6 is not important. Rather, the competing many-body effect enhancement becomes the most prominent feature in their experiment.

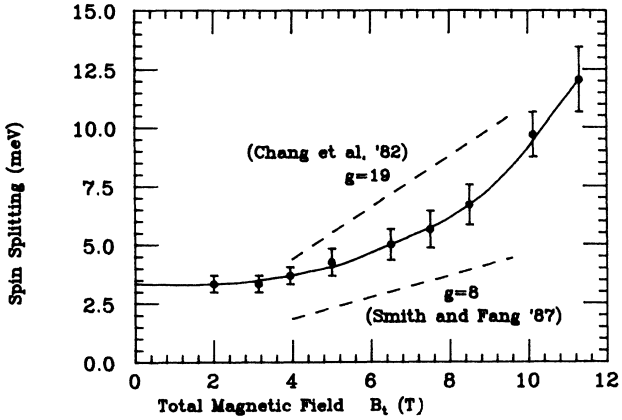

FIG. 8. The spin splitting as a function of the total magnetic field. Note that the spin splitting has little field dependence for $B_t<5.0$ T and then increases nonlinearly beyond that field. The dashed lines show the spin Zeeman splitting for $g=8$ and 19.

The monotonic increase of the spin splitting with magnetic field suggests that the zero-field spin splitting and Zeeman splitting enhance each other in this sample. How the zero-field spin splitting relates to the field-induced Zeeman splitting provides another clue to distinguish whether it is originated from the bulk asymmetry or the surface electric field. According to the calculation by Lommer *et al.*,[16] the surface-field-induced zero-field splitting has the same sign as the Zeeman splitting, whereas the bulk-asymmetry-induced spin splitting has the opposite sign. For GaAs quantum wells dominated by bulk asymmetry, the spin splitting is predicted to decrease first as the magnetic field increases from zero, vanishing at a finite magnetic field, and only to increase with magnetic field when the Zeeman term is larger than the bulk term. The measured spin splitting shown in Fig. 8, however, does not go to zero at any magnetic fields. Lommer *et al.* also pointed out that the spin-orbit term is expected to become more important for the inversion layers on the narrow-gap semiconductors, such as InSb and $Hg_xCd_{1-x}Te$. Our system InAs, very much like InSb in

terms of band parameters, certainly falls into this group of narrow-gap systems. Thus, the observed field dependence of the spin splitting supports our previous conclusion that the surface electric field is the origin of the zero-field splitting in the InAs/GaSb quantum wells.

V. THE POSSIBILITY OF SPIN-DEPENDENT SCATTERING

The final discussion concerns the scattering of the 2D electrons in the quantum well. At a given temperature, the SdH oscillation amplitude of ρ_{xx} due to collision damping is[17]

$$A \sim \omega_c^3 \exp\left[-\frac{\pi}{\omega_c \tau}\right], \tag{13}$$

where τ is the single-particle relaxation time which in general is closely related to the electron scattering time. In the case of our experiment, there are two sets of SdH oscillations contributing to the measured oscillatory resistivity. The line shape of the beating pattern in the data relates to the amplitudes (A_1, A_2) of the two SdH components: the extrema of the beat amplitude are given by $A_1 - A_2$ and $A_1 + A_2$. Thus the electron scattering of the two spin subbands can be compared with each other through the amplitude analysis of the beat patterns.

We first consider the 75-Å well. In small magnetic fields, for example Fig. 1(a), the vanishing oscillation amplitudes at the beat nodes suggest that the electrons from the two spin subbands oscillate with equal strength, or their scattering times are equal. In strong magnetic field, the two scattering times become so different that only one band contributes to the oscillations at low perpendicular field. This is clearly illustrated by the $B_t = 11.3$ T data shown in Fig. 7, from which we also determined that the low-energy spin state has a much longer scattering time than the high-energy state. The change in the relative scattering time is a gradual one as shown by Fig. 6, where the beat node amplitude increases as the total magnetic field is increased. It should be noted that since the electron concentrations are not equal for the two spins, their SdH oscillation amplitudes are different even if the two scattering times are the same. However, this effect is small, and the changes in the beat amplitudes are caused mostly by the changes in the electron scattering times.

The observation of the different scattering times for the two spin subbands is not limited to the presence of a parallel magnetic field, which effectively increases the spin splitting. Nonzero node amplitudes are also shown in Fig. 1(b) by the 100-Å sample whose zero-field spin splitting is about four times larger than that of the 75-Å well due to a strong built-in electric field. Therefore, there seems to be a close link between the energy separation of the two spin states and their scattering time difference; how the spin splitting is introduced, i.e., by an interface electric field or by an external magnetic field, might be of less importance. A spin-dependent scattering process which suppresses the SdH oscillation of one spin more than the other is needed to explain our observations. We are not aware of any scatters in our system which may give nonequivalent scatterings for the two spin states. However, one might speculate that the paramagnetism of the charged scatters at high magnetic field might play a role. The magnetic field dependence of the SdH amplitude is frequently used to deduce the electron scattering time. In our case this becomes rather difficult because the two sets of SdH oscillations are superimposed. Other qualitative measurements on the electron scattering times should be conducted before we can understand the details of the scattering mechanisms.

In addition to growing apart from each other, the two scattering times also show an overall decrease with the increasing external magnetic field. The scattering time can also be estimated from the value of the lowest quantizing field at which the oscillation can be resolved. The so-called on-set field requires that $\omega_c \tau \simeq 1$, or is inversely proportional to the electron scattering time. We observed that the on-set field of the oscillations, which is determined by the longer one of the two scattering times involved, moves up to higher quantizing field $B_\perp$ as the total magnetic field is increased. Since the field window in $B_\perp$ is roughly fixed for all tilted field data, an increase of total magnetic field is equivalent to an increase of the parallel magnetic field component. The overall decrease of the electron scattering times is attributed to the parallel-field-induced Lorentz force which pushes electrons in the 2D layer towards the interfaces of the quantum well. As a result, the scattering of the electrons by the interface roughness and by charged centers located near the interfaces is enhanced.

To quantitatively illustrate this point, we measured longitudinal resistivity by applying the magnetic field strictly parallel to the well plane. The results in Fig. 9 show a drastic increase of the longitudinal resistivity as soon as the field is turned on. The fact that the beating patterns in Fig. 6 at $B_t = 2.0$, 3.1, and 4.0 T have zero node amplitude suggests the two spin bands have about the same scattering times in small magnetic field ($B_t < 4$

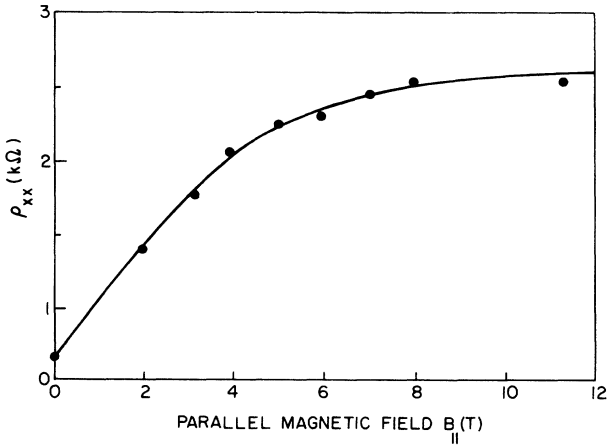

FIG. 9. The magnetoresistance as a function of the parallel magnetic field. Since ρ_{xx} is inversely proportional to the averaged electron scattering time τ, this result shows that τ decreases with the parallel field due to increased electron scattering.

T). The positive magnetoresistance in this field region can only come from the enhanced surface scattering as the result of deformation of the electron wave function in the presence of the parallel magnetic field. For the intermediate field of about 4 to 7 T, we have an additional contribution to the observed positive magnetoresistance because the scattering times of the two spin bands become different. For a two-carrier system, one always observes a positive magnetoresistance which is proportional to the square of the difference of the two scattering times.[18] It is quite interesting to note that the measured magnetoresistance in Fig. 9 saturates for fields above 7 T as if the system behaves as a single carrier system again. This is due to the fact that one of the spin bands has diminishing mobility at high magnetic fields.

VI. CONCLUSIONS

Between the two sources of inversion asymmetry existing in the InAs/GaSb quantum wells, i.e., that of the InAs bulk structure and that of the confining potential, we have shown that the latter dominates the 2D electron energy band structures for the samples studied. The electron Landau-level spectrum in small perpendicular external magnetic field is found to be best described by Rashba's calculation that includes the spin-orbit term $H_{s.o.}=\alpha_s(\sigma\times\mathbf{k})\cdot\mathbf{z}$ into the electron Hamiltonian. We found that the spin splitting of the ground electron subband does not vanish at $B=0$, and increases nonlinearly with the increase of the external magnetic field. This is the combined result of the surface electric-field-induced spin splitting and the external magnetic-field-induced spin Zeeman splitting. We also observed that the difference between the quantum scattering times of the two spin states increases with their energy separation, i.e., the spin splitting. The electrons in the low-energy spin states are found to have a longer scattering time than those of the high-energy spin states. The details of the spin-dependent scattering mechanism are not clear at present.

ACKNOWLEDGMENTS

The technical assistance of J. Nocera is gratefully acknowledged. This work was supported in part by National Science Foundation (NSF) Grant No. DMR-87-17817.

*Present address: Francis Bitter National Magnet Laboratory, Cambridge, MA 02139.

[1]For a review, see Tsuneya Ando, Alan B. Fowler, and Frank Stern, Rev. Mod. Phys. **54**, 551 (1982).

[2]D. Stein, K. v. Klitzing, and G. Weimann, Phys. Rev. Lett. **51**, 130 (1983).

[3]B. Das, D. C. Miller, R. Reifenberger, S. Datta, W. P. Hong, P. K. Bhattacharya, J. Singh, and M. Jaffe, Phys. Rev. B **39**, 1411 (1989).

[4]Ulrich Rössler, Franz Malcher, and Gerhard Lommer, in *Proceedings of the International Conference on the Application of High Magnetic Field in Semiconductor Physics, 1988, Wurzburg,* edited by G. Landwehr (Springer-Verlag, Berlin, 1989), p. 214.

[5]L. L. Chang, E. E. Mendez, N. J. Kawai, and L. Esaki, Surf. Sci. **113**, 306 (1982).

[6]T. P. Smith and F. F. Fang, Phys. Rev. B **35**, 7729 (1987).

[7]J. Luo, H. Munekata, F. F. Fang, and P. J. Stiles, Phys. Rev. B **38**, 10 142 (1988).

[8]G. Dresselhaus, Phys. Rev. **100**, 580 (1955).

[9]R. Eppenga and M. F. H. Schuurmans, Phys. Rev. B **37**, 10 923 (1988).

[10]E. I. Rashba, Fiz. Tverd. Tela (Leningrad) **2**, 1224 (1960) [Sov. Phys.—Solid State **2**, 1109 (1960)].

[11]Yu. A. Bychkov and E. I. Rashba, Pis'ma Zh. Eksp. Teor. Fiz. **39**, 66 (1984) [JETP Lett. **39**, 78 (1984)].

[12]T. Englert, D. Tsui, A. Gossard, and C. Uihlein, Surf. Sci. **113**, 295 (1982).

[13]T. Ando and Y. Uemura, J. Phys. Soc. Jpn. **36**, 959 (1974).

[14]F. F. Fang and P. J. Stiles, Phys. Rev. **174**, 823 (1968).

[15]V. F. Radantsev, T. I. Deryabina, L. P. Zverev, G. I. Kulaev, and S. S. Khomutova, Zh. Eksp. Teor. Fiz. **88**, 2088 (1985) [Sov. Phys.—JETP **61**, 1234 (1985)].

[16]G. Lommer, F. Malcher, and U. Rössler, Phys. Rev. Lett. **60**, 728 (1988).

[17]F. F. Fang, T. P. Smith, and S. L. Wright, Surf. Sci. **196**, 310 (1988).

[18]See, for example, R. A. Smith, *Semiconductors* (Cambridge University Press, Cambridge, 1976), p. 214.